Appendix G. Scanning Electron Microscope (SEM) and Electron Microprobe (EMPA) Analyses at Queen's University of Rock Core Samples from the Kiggavik Uranium Deposit, Nunavut

Introduction

Samples analyzed under the Scanning Electron Microscope (SEM) and Electron Microprobe (EMPA) at Queen's University were selected on the basis that they might contain mineralogy that uniquely characterizes the Kiggavik style of unconformity-associated uranium deposits. The importance of documenting this mineralogy is to characterize the deposits and thereby calibrate the heavy mineral concentrate (HMC) recovered by Overburden Drilling Management (ODM) from the till samples collected around the deposit. Ultimately, the purpose of this work is to characterize and delineate an indicator mineral suite that is unique to unconformity-associated uranium deposits that may be applicable for exploration in glaciated terrains.

SEM and EMPA analyses focused on samples that have a minimum of 300 counts per second (cps) of gamma radiation, which indicates that the sample may have at least a minor elevated uranium composition. Furthermore, samples that display "illite" alteration (illite +/- chlorite) were also examine under the SEM and EMPA to document and quantify their mineralogy and compositions, although the focus is on potentially transportable heavy minerals rather than clay.

Review of the mineralogy of uraniferous samples led to an unexpected discovery. Apatite crystals with lead contents in the range of 0 to8 wt% PbO and uranium contents in the range of 0 to 1.7 wt% UO_2 were observed under SEM, and followed up by EMPA. This discovery potentially has significant implications for geochronological constraints on mineralization and for use of these apatite grains as silt-sized indicator minerals for the Kiggavik style of unconformity-associated uranium deposits.

Due to limited time and minimal returns from the normal sand-size HMC obtained from bulk till samples, only three minerals were quantitatively analyzed by EMPA. Uraninite, coffinite and Pb-apatite were selected on the basis that they can potentially be used as indicator minerals if they can be efficiently and effectively separated as HMC from the <100 μm fraction. Table G-1 shows the distribution of 38 spot analyses from 5 different samples containing uraninite/coffinite and another 38 spot analyses of Pb-apatite in 2 samples.

Table G-1. List of seven samples examined under SEM, and numbers of spots analyzed on six samples by EMPA (Table G-2). UO = uraninite and coffinite. Pb-A = fluorapatite enriched in U and Pb.

Samples 10PTA-R	Drill-hole, depth (m)	Figures in this report	# spots (UO)	# spots (Pb-A)
045	MZ-LG241, 134	1	1	nil
046	MZ-LG241, 40.4	2	2	nil
050	MZ-LG241, 144	10-15	nil	24
051	MZ-LG271, 45.1	3	1	nil
053	MZ-LG271, 68.5	4, 5, 16	2	14
063	MZ-LG208, 85.3	6, 7, 8, 9	32	nil
064	MZ-LG264, 86.8	na	nil	nil

Uranium oxide minerals and lead- +uranium-rich apatite

Uraninite is the dominant uranium phase examined by SEM and EMPA in this study. Two samples (10-PTA-R063 and to a lesser degree 10-PTA-R064) have higher overall CPS, are clearly mineralized to the naked eye, and contain more than 50% uraninite. In these samples, most of the uraninite is coarsely crystalline (>2000 μm) and densely disseminated to massive, transected by multiple intersecting veinlets of calcite and quartz+calcite.

Samples with a lower CPS, yet still uraniferous, display a more vein-like, elongated stringer texture or very finely crystalline intergrowth with and/or replacement of phyllosilicate minerals (samples 10-PTA-R045, 046, 050, 051, and 053). These textures are also a minor part of sample 10-PTA-R064. Given the intergrowth and/or inclusion textures, the high SiO_2 content measured by EMPA in some "uraninite" patches may be interpreted as a result of silicate inclusions in the UO_2 or as the presence of coffinite. Fine crystals (20–50 μm) of relatively pure uraninite are also disseminated in the samples, located near the centres of the uraninite-silicate intergrowth patches.

To reduce the time required for analyses, each spot analysis of a uranium-bearing mineral was limited to a selection of 10 elements, which are reported as oxides (SiO_2, Al_2O_3, CaO, FeO, UO_2, ThO_2, Na_2O, Y_2O_3, PbO, P_2O_5), and constitute approximately 90% of the bulk chemical composition (Table G-2).

Table G-2. Spot analyses of uranium oxide minerals by microprobe, arranged in order of figure number and numbered spots on those figures. Ten selected elements are reported as weight % oxide.

Figure -spot	Samples 10-PTA-R	SiO_2	Al_2O_3	CaO	FeO	UO_2	ThO_2	Na_2O	Y_2O3	PbO	P_2O_5	Total (%)
1-1	045-MP1	7.34	na	0.92	na	80.67	na	0.00	0.01	0.20	na	89.15
2-1	046-MP1	5.22	na	3.51	na	80.29	na	0.00	0.01	0.22	na	89.25
2-2	046-MP1	5.34	na	3.86	na	81.02	na	0.01	0.00	0.02	na	90.25
3-1	051-MP-1	1.03	0.49	2.11	1.14	79.81	0.01	0.26	0.08	0.18	3.24	88.36
4-2	053-MP-1	4.31	0.80	3.32	0.53	63.49	0.00	0.07	0.56	0.11	1.33	74.51
5-1	053-MP-2	1.51	na	4.94	na	74.57	na	0.01	0.07	0.02	na	81.12
6-1	063-MP-1	1.81	0.13	5.58	0.47	82.50	0.00	0.75	0.11	4.16	0.08	95.60
6-2	063-MP-1	1.98	0.15	5.40	0.51	82.90	0.00	0.73	0.12	4.40	0.09	96.27
6-3	063-MP-1	1.96	0.18	5.43	0.51	83.00	0.00	0.66	0.08	4.49	0.08	96.40
6-4	063-MP-1	2.03	0.18	5.31	0.51	83.63	0.00	0.81	0.08	4.16	0.09	96.81
6-5	063-MP-1	1.90	0.16	5.77	0.49	82.57	0.00	0.67	0.05	4.12	0.08	95.81
6-6	063-MP-1	2.04	0.14	5.55	0.56	82.34	0.01	0.69	0.12	4.21	0.09	95.75
6-7	063-MP-1	2.08	0.28	5.06	0.51	82.45	0.00	0.89	0.11	5.13	0.09	96.60
6-8	063-MP-1	1.58	0.11	6.08	0.39	83.01	0.00	0.65	0.08	4.44	0.08	96.42
7-1	063-MP-2	1.69	0.12	5.75	0.41	82.55	0.00	0.64	0.08	3.98	0.04	95.27
7-2	063-MP-2	1.86	0.14	5.83	0.46	82.61	0.00	0.71	0.07	3.92	0.07	95.65
7-3	063-MP-2	2.14	0.19	5.30	0.50	82.12	0.00	0.94	0.12	3.95	0.08	95.32
7-4	063-MP-2	1.98	0.22	5.21	0.47	82.30	0.00	0.79	0.08	4.16	0.09	95.31
7-5	063-MP-2	2.24	0.19	5.78	0.52	82.46	0.00	0.74	0.09	4.28	0.08	96.37
7-6	063-MP-2	1.92	0.15	5.46	0.51	83.39	0.00	0.65	0.10	3.90	0.10	96.18
7-7	063-MP-2	1.87	0.21	5.43	0.49	82.55	0.00	0.53	0.11	4.03	0.11	95.33
7-88	063-MP-2	2.02	0.17	5.51	0.44	82.87	0.01	0.63	0.07	4.21	0.10	96.03
8-1	063-MP-3	14.97	0.36	3.43	0.55	60.68	0.00	0.03	0.25	4.97	0.16	85.41
8-2	063-MP-3	14.24	0.16	3.51	0.59	60.85	0.00	0.02	0.17	3.80	0.18	83.51
8-3	063-MP-3	15.08	0.23	3.25	1.32	54.50	0.00	0.01	0.23	6.08	0.15	80.85
8-4	063-MP-3	15.36	0.24	3.57	1.39	57.93	0.00	0.01	0.25	5.82	0.15	84.73
8-5	063-MP-3	13.94	0.92	2.74	0.50	53.47	0.00	0.01	0.14	14.3	0.13	86.14
8-6	063-MP-3	15.26	0.23	3.18	0.11	59.21	0.00	0.02	0.16	5.48	0.13	83.78
8-7	063-MP-3	15.62	0.20	3.74	2.39	57.16	0.00	0.05	0.18	3.79	0.12	83.25
8-8	063-MP-3	15.56	0.21	3.76	1.84	59.25	0.00	0.06	0.14	3.74	0.16	84.71
9-1	063-MP-4	2.29	0.25	4.83	0.44	82.46	0.00	0.82	0.09	4.53	0.09	95.79
9-2	063-MP-4	2.45	0.28	5.31	0.51	81.59	0.00	0.78	0.06	4.60	0.09	95.68
9-3	063-MP-4	2.15	0.19	5.32	0.58	82.79	0.00	0.80	0.08	3.91	0.06	95.89
9-4	063-MP-4	2.27	0.27	5.06	0.56	82.08	0.00	0.95	0.09	4.02	0.06	95.35
9-5	063-MP-4	2.43	0.29	4.40	0.40	82.15	0.00	0.74	0.08	4.77	0.11	95.38
9-6	063-MP-4	4.88	0.96	5.39	1.29	63.87	0.00	0.32	0.32	8.47	0.15	85.66
9-7	063-MP-4	2.07	0.25	5.40	0.48	83.18	0.00	0.71	0.08	4.18	0.10	96.46
9-8	063-MP-4	2.65	0.36	4.40	0.43	81.11	0.00	0.87	0.09	4.61	0.15	94.67

Photomicrographs showing representative textures and the locations of spot analyses by EMPA (Table G-2).

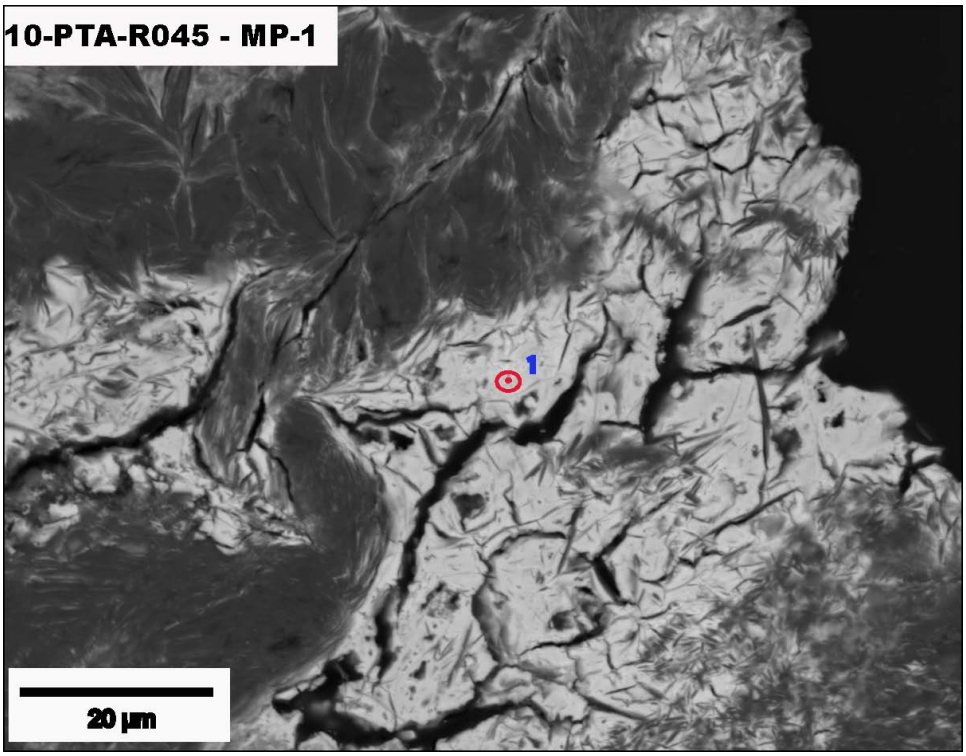

Figure G-1. 10-PTA-R045 - MP-1. Uraninite (analyzed at spot 1) enclosing and intermingled with "illite" (the grey feathery textured surroundings).

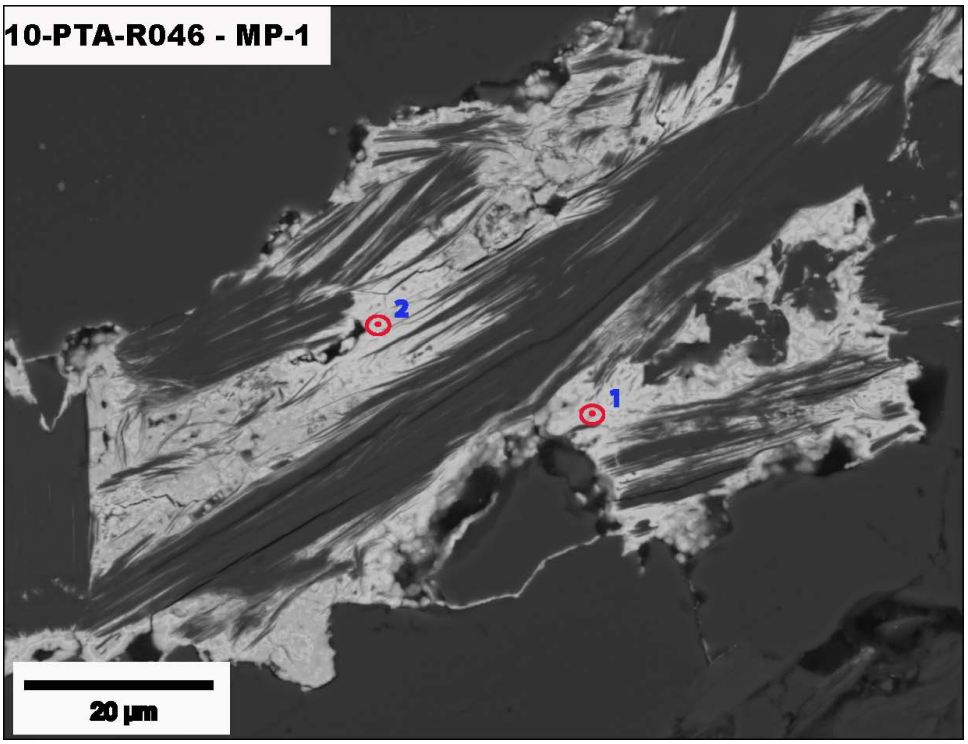

Figure G-2. Uraninite (analyzed at spots 1 and 2) that has been partially replaced and enclosed by muscovite along foliation planes. Dark grey uniform minerals at upper left and lower right are mainly quartz and feldspar.

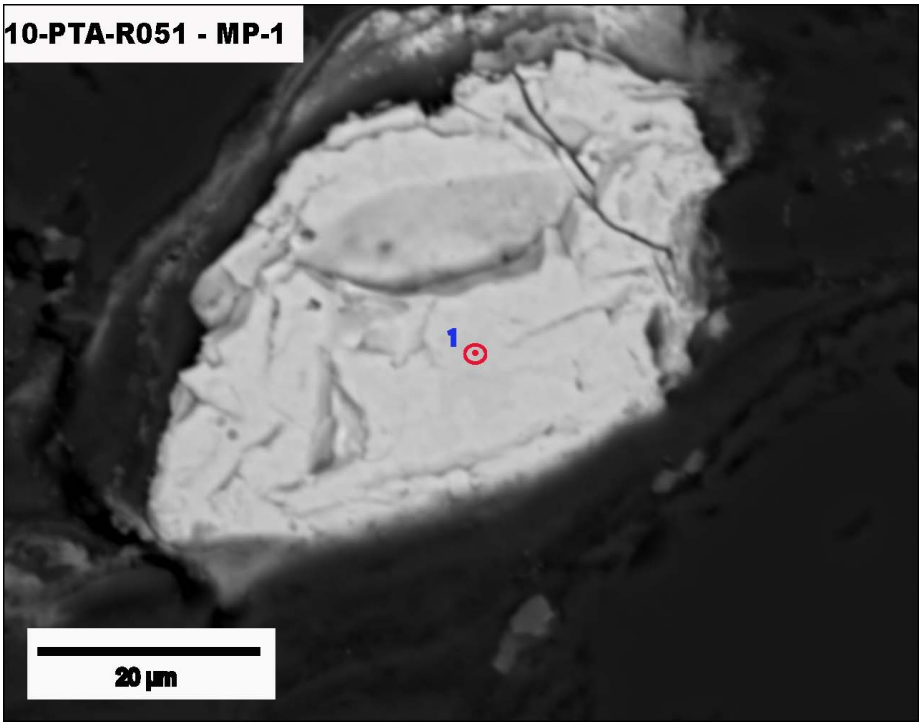

Figure G-3. Finely crystalline, anhedral uraninite analyzed at spot 1, enclosed by quartzofeldspathic minerals.

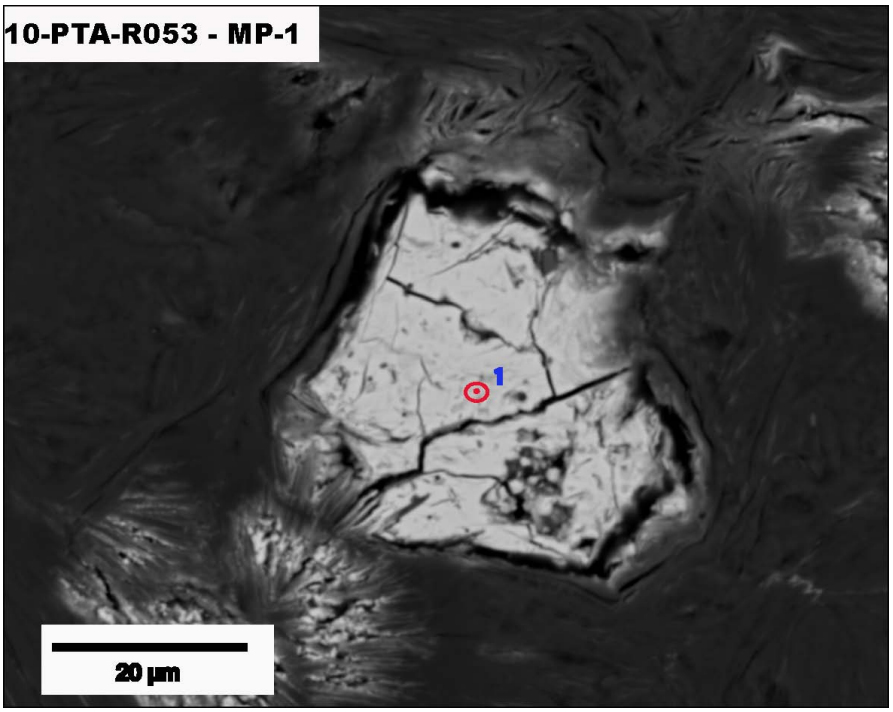

Figure G-4. A small crystal of subhedral blocky uraninite analyzed at spot 1, enclosed by felted illite (medium grey) that contains uraniferous (light grey) radiating illite patches.

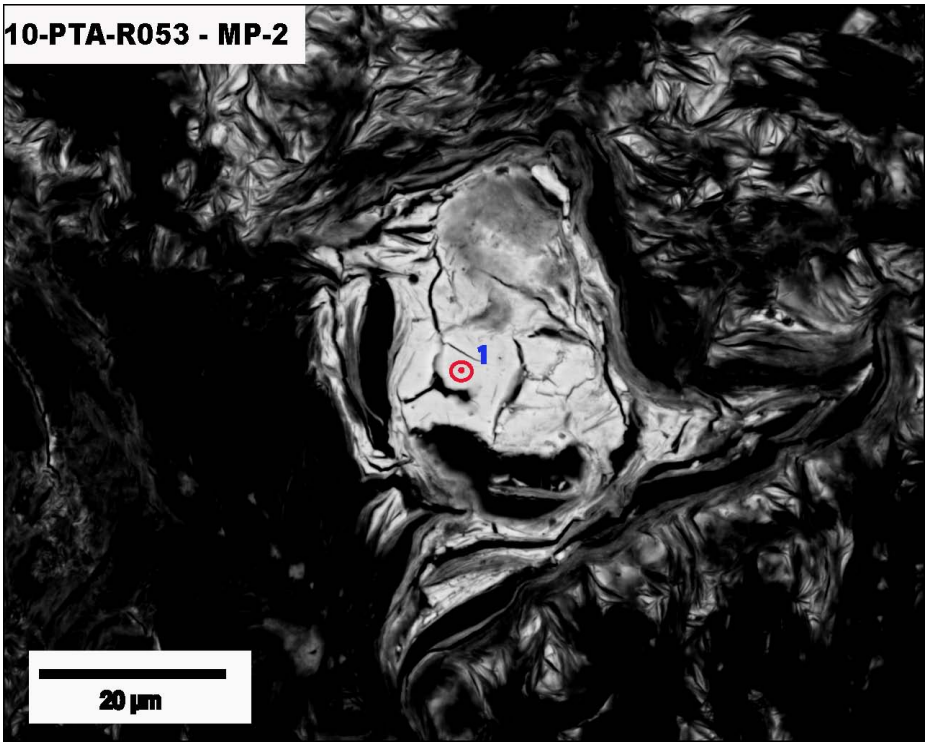

Figure G-5. Small crystal of subhedral uraninite within and partially enclosing felted mass of illite which is oriented overall randomly but sub-parallel to and frames the uraninite grain boundary. An unresolvable uranium phase also occupies the matrix within the illite mass.

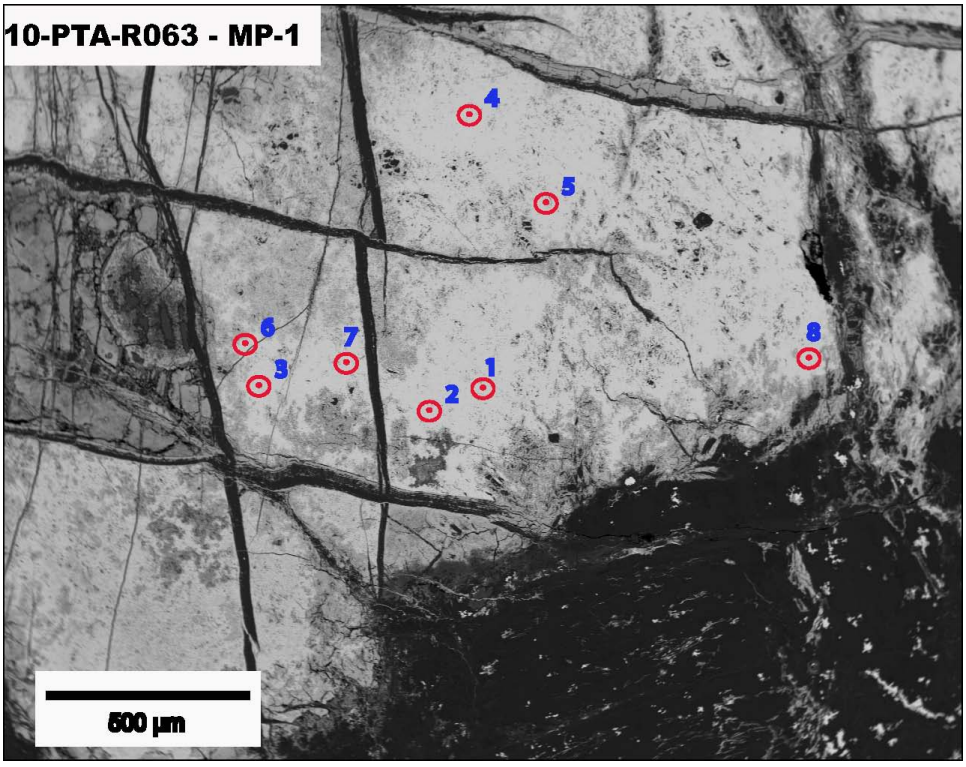

Figure G-6. Coarsely crystalline, massive uraninite transected by sub-orthogonal fractures filled by calcite (medium grey) and quartz (dark grey) +calcite. The matrix was not analyzed.

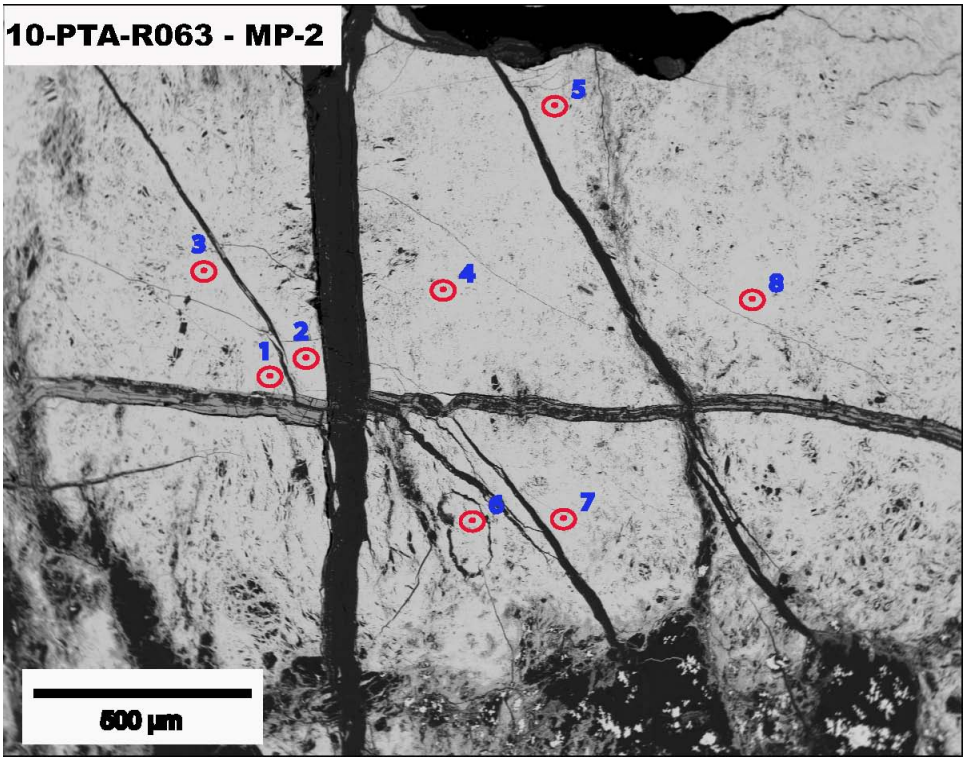

Figure G-7. Coarsely crystalline, massive uraninite crosscut by orthogonal and oblique laminated (crack-seal) calcite veins.

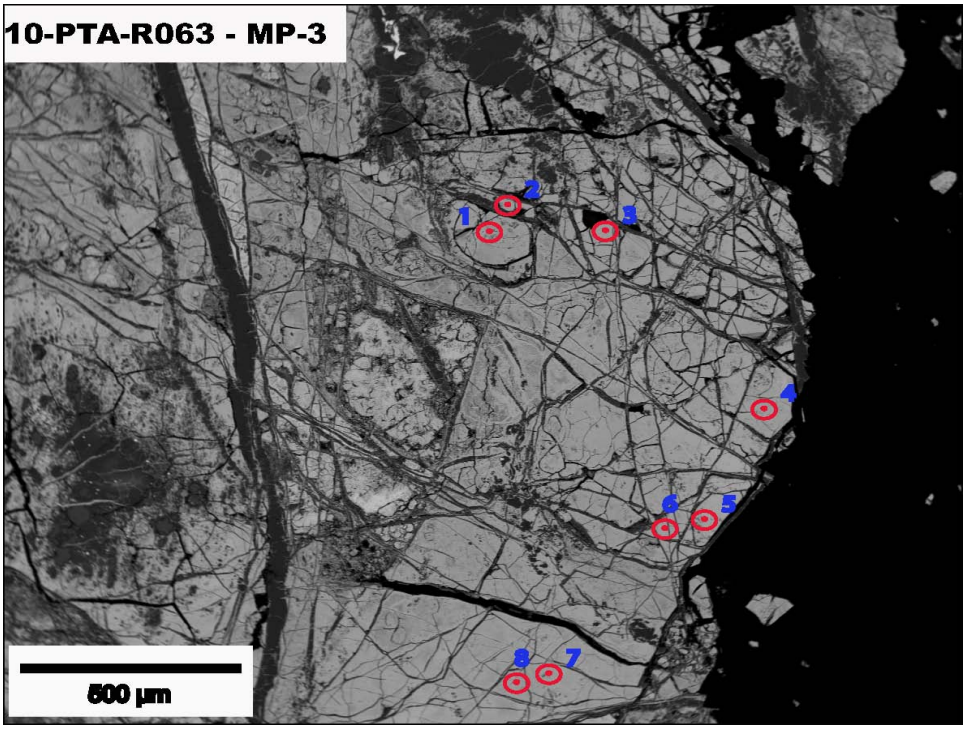

Figure G-8. Coarsely crystalline coffinite (13.9–15.6% SiO_2) cut by quartz and calcite veinlets. This has lower reflectance than the uraninite shown in Figure 7. The black area on right is epoxy.

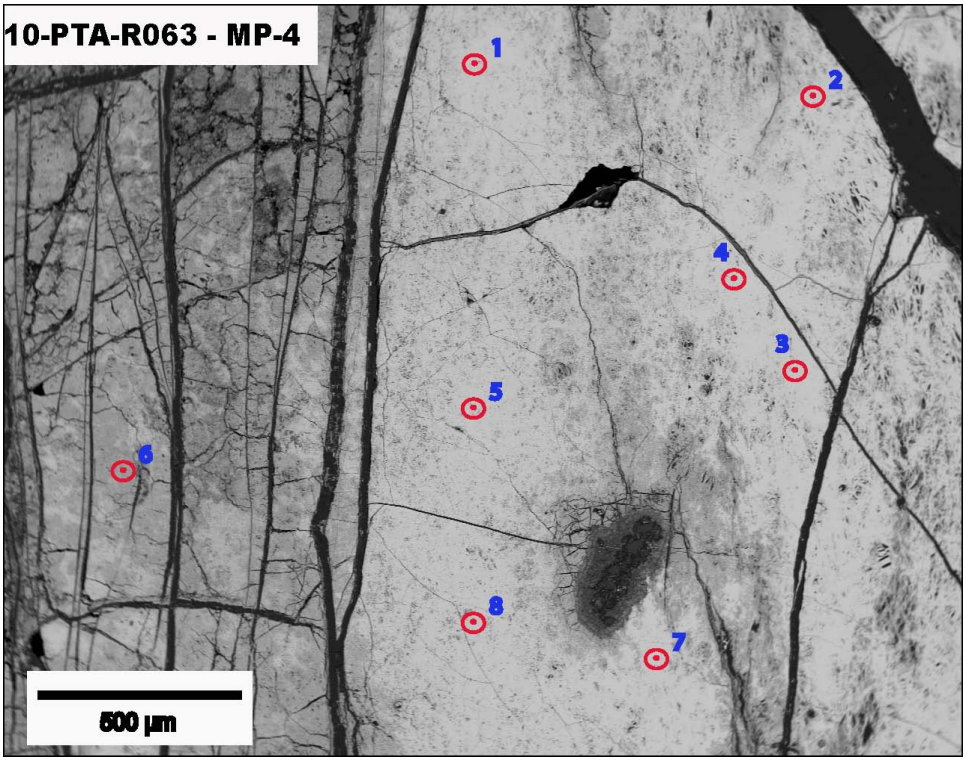

Figure G-9. Coarsely crystalline uraninite transected by quartz and calcite veinlets.

Pb+U - apatite chemistry and context

The apatite crystals that contain lead were discovered in highly altered, weakly uraniferous, foliated metagreywacke. They are interstitial to and partly replace relict 20–200 μm lath-shaped cross sections of muscovite plates that record the primary metamorphic foliation. These are surrounded by moderate to strong illite alteration with minor hematite/limonite. The replacement texture of phyllosilicates includes both random and preferred orientations. Uraninite ranges in habit from very finely crystalline disseminations within the felted phyllosilicates, through finely crystalline anhedra to subhedra, to very coarsely crystalline masses. The term "illite" is used as a general term for captions based on comparison with petrographic data on similar samples and other work in the camp (e.g. Miller and LeCheminant, 1985; Paquette 1993; Reyx, 1994; Riegler et al., 2015; Sharpe et al., 2015), however this study did not focus on identification of phyllosilicates therefore the phases labelled illite may include chlorite.. Notably, apatite is not present in samples where uraninite and coffinite constitute over 50% of the rock.

Apatite crystals containing lead were analyzed by EMPA to quantify the Pb and U at representative spots in each individual grain and to observe the variability in composition compared to typical apatite $Ca_5(PO_4)_3(OH,F,Cl)$. Not all apatite crystals in weakly mineralized specimens from Kiggavik contain Pb, however elevated Pb is very common amongst those crystals that fit the criteria mentioned above. Microprobe analyses of 38 spots were distributed over multiple crystals in two samples (10-PTA-R050 and 10-PTA-R053). From the analyses, the weight % masses of a wide suite of selected elements (Table G-3) were calculated. Lead-enriched apatite crystals were also observed in samples 10-PTA-R045, 10-PTA-R046, and 10-PTA-R051, although these were not analyzed by EMPA.

Figures G-10 to G-12, G-16, and G-17 show where representative spots were analyzed by EMPA to calculate weight % oxide. These images, together with those in Figures 18 and 19, also illustrate the textures and structural context of apatite, uraninite, and phyllosilicate crystals. Apatite paragenesis appears to be closely related to hydrothermal alteration products: illite, chlorite, and uraninite, all of which, including apatite, are dominantly interstitial to, but partly replace the muscovite. Some apatite crystals include oriented laths of illite or sericite, and their outer replacement or overgrowth rims contain a lamellar grain that is closely aligned with that of enclosing illite. Furthermore, the Pb-apatite grains are commonly spatially associated with finely crystalline anhedral pyrite (Fig. G-10) and associated wispy limonite and stringers of secondary uranium minerals surrounding uraninite.

The Pb content of the apatite crystals (Table G-3) varies from 0 to 8.06% PbO, with the average PbO being 2.17%. These variations are replicated by the UO_2 values, both being in the outer rims of the apatite and concomitant with depletion of Ca (Figs. G-13, G-14, and G-15). Zones of the apatite crystals that have higher Pb concentrations are represented by a higher reflectance (brighter colours) in Figures G-10 to G-12 and G-16 to G-19, inclusive.

Further work is needed to properly assess the abundance of Pb-apatite in Kiggavik and other similar systems, and whether or not this mineral is diagnostic of a specific type of deposit. One reason for the Pb enrichment could be that the apatite crystals were first enriched in U, after which Pb was produced by radioactive decay. This hypothesis could be tested by determining whether the Pb is radiogenic.

Table G-3. Thirty-eight spot geochemical analyses by EMPA of apatite crystals illustrated in Figures G-10 to G-19, inclusive, for samples 10-PTA-R050 and 10-PTA-R053. Values are expressed as weight % of selected elements as oxides. Analyzed spots are labelled on the photomicrographs and linked to this table by figure - spot number. The designations a1, a2 and a3 under the Sample column refer to different apatite grains in the same sample, which are shown in successive figures. Analyses of the apparently least-altered portions (based on colour and texture variations in the photomicrographs) of the apatite crystals are shaded in grey.

Fig.-Pt.	Sample 10PTAR-	F	SiO_2	Gd_2O_3	Sm_2O_3	Nd_2O_3	Pr_2O_3	La_2O_3	P_2O_5	CaO	Cl	ThO_2	Na_2O_3	UO_2	PbO	Y_2O_3	Ce_2O_3	Total	O=F	Total
10-1	050 a1	3.64	0.06	0.17	0.14	0.41	0.09	0.03	38.30	48.07	0.00	0.45	0.15	**0.91**	**8.06**	0.27	0.02	100.76	1.53	99.23
10-2	050 a1	4.49	0.08	0.00	0.34	0.00	0.00	0.00	38.87	49.41	0.00	0.00	0.12	**1.43**	**5.37**	0.28	0.15	100.55	1.89	98.66
10-3	050 a1	3.91	0.07	0.00	0.00	0.19	0.00	0.13	38.41	50.95	0.00	0.06	0.03	**1.20**	**3.45**	0.13	0.01	98.53	1.65	96.89
10-4	050 a1	4.79	0.04	0.00	0.04	0.05	0.17	0.00	39.49	55.10	0.00	0.05	0.03	**0.02**	**0.43**	0.12	0.01	100.33	2.02	98.31
10-5	050 a1	4.60	0.05	0.00	0.07	0.17	0.01	0.00	39.76	55.08	0.01	0.02	0.05	**0.07**	**0.47**	0.21	0.04	100.62	1.94	98.68
10-6	050 a1	4.10	0.08	0.06	0.20	0.34	0.00	0.00	38.23	54.54	0.01	0.17	0.02	**0.08**	**0.33**	0.07	0.06	98.30	1.73	96.57
10-7	050 a1	4.22	0.07	0.11	0.00	0.12	0.00	0.00	42.53	55.89	0.00	0.00	0.00	**0.01**	**0.00**	0.03	0.00	102.98	1.78	101.20
10-8	050 a1	3.94	0.09	0.02	0.04	0.02	0.14	0.00	38.68	48.72	0.00	0.33	0.13	**1.33**	**5.96**	0.24	0.02	99.66	1.66	98.00
10-9	050 a1	5.63	0.27	0.06	0.05	0.11	0.07	0.06	39.00	54.90	0.00	0.08	0.05	**0.12**	**0.55**	0.23	0.02	101.20	2.37	98.83
10-10	050 a1	3.86	0.09	0.03	0.13	0.00	0.03	0.00	42.42	55.59	0.01	0.00	0.01	**0.00**	**0.00**	0.00	0.00	102.16	1.63	100.53
11-1	050 a2	4.00	0.00	0.11	0.03	0.00	0.09	0.00	43.09	53.58	0.02	0.00	0.06	**0.03**	**0.01**	0.06	0.13	101.20	1.68	99.52
11-2	050 a2	3.80	0.03	0.01	0.00	0.10	0.00	0.17	39.18	50.22	0.00	0.57	0.13	**1.06**	**3.86**	0.20	0.11	99.45	1.60	97.85
11-3	050 a2	3.87	0.94	0.00	0.06	0.13	0.04	0.15	37.86	49.70	0.00	1.03	0.23	**1.71**	**2.23**	0.16	0.03	98.13	1.63	96.50
11-4	050 a2	3.71	0.04	0.00	0.00	0.00	0.00	0.00	40.11	52.70	0.00	0.02	0.04	**0.42**	**2.17**	0.00	0.10	99.31	1.56	97.74
11-5	050 a2	4.92	0.07	0.26	0.09	0.00	0.06	0.02	39.95	52.79	0.00	0.26	0.06	**0.16**	**0.85**	0.14	0.00	99.63	2.07	97.56
12-1	050 a3	2.84	0.17	0.06	0.00	0.10	0.12	0.09	42.17	53.56	0.02	0.00	0.14	**0.03**	**0.04**	0.18	0.02	99.55	1.20	98.35
12-2	050 a3	2.94	0.22	0.03	0.00	0.00	0.10	0.10	38.36	48.54	0.01	0.06	0.17	**1.63**	**5.60**	0.31	0.00	98.07	1.24	96.83
12-3	050 a3	3.23	1.35	0.13	0.09	0.03	0.11	0.05	38.03	48.84	0.00	0.00	0.16	**1.36**	**4.54**	0.24	0.08	98.25	1.36	96.89
12-4	050 a3	3.53	0.20	0.26	0.00	0.00	0.00	0.05	39.23	51.18	0.00	0.01	0.14	**1.25**	**4.34**	0.17	0.13	100.49	1.49	99.01
12-5	050 a3	4.16	0.44	0.02	0.15	0.23	0.08	0.00	39.11	53.72	0.01	0.08	0.06	**0.32**	**0.89**	0.14	0.01	99.42	1.75	97.67
12-6	050 a3	3.59	0.35	0.12	0.15	0.00	0.00	0.03	38.45	48.97	0.00	0.15	0.14	**1.44**	**5.62**	0.20	0.12	99.32	1.51	97.81
12-7	050 a3	3.51	0.43	0.07	0.03	0.05	0.06	0.00	39.65	49.20	0.00	0.26	0.18	**1.22**	**5.13**	0.23	0.09	100.09	1.48	98.61
12-8	050 a3	4.34	0.06	0.00	0.00	0.11	0.00	0.00	41.46	54.10	0.01	0.08	0.02	**0.00**	**0.91**	0.03	0.00	101.12	1.83	99.29
12-9	050 a3	3.08	0.04	0.00	0.24	0.02	0.04	0.00	42.15	53.62	0.10	0.03	0.05	**0.00**	**0.01**	0.08	0.05	99.52	1.30	98.23
16-1	053 a1	4.65	0.02	0.34	0.34	1.19	0.19	0.09	37.51	49.34	0.00	0.00	0.21	**1.20**	**2.38**	0.30	0.11	97.89	1.96	95.93
16-2	053 a1	5.04	0.03	0.30	0.30	0.88	0.25	0.22	36.92	50.28	0.01	0.04	0.12	**0.95**	**1.90**	0.32	0.15	97.71	2.12	95.59
16-3	053 a1	3.67	0.04	0.01	0.04	0.00	0.04	0.11	41.88	54.09	0.01	0.04	0.08	**0.00**	**0.02**	0.11	0.05	100.19	1.55	98.64
16-4	053 a1	3.24	0.04	0.09	0.04	0.14	0.05	0.03	42.78	54.45	0.01	0.02	0.07	**0.00**	**0.00**	0.21	0.00	101.16	1.36	99.80
16-5	053 a1	4.27	0.03	0.13	0.25	0.72	0.25	0.11	36.62	51.88	0.03	0.04	0.17	**0.78**	**1.67**	0.24	0.14	97.34	1.80	95.54
16-6	053 a1	3.96	0.02	0.37	0.30	1.36	0.24	0.00	36.95	49.58	0.01	0.00	0.16	**1.29**	**2.45**	0.27	0.13	97.10	1.67	95.43
16-7	053 a1	3.35	0.06	0.27	0.38	1.27	0.22	0.07	37.29	49.11	0.00	0.00	0.26	**1.11**	**2.35**	0.24	0.14	96.10	1.41	94.69
16-8	053 a1	4.90	0.08	0.43	0.17	0.90	0.00	0.07	36.41	50.51	0.01	0.05	0.21	**0.90**	**1.76**	0.25	0.06	96.69	2.06	94.63
17-1	053 a2	3.75	0.04	0.00	0.00	0.17	0.00	0.12	42.24	54.26	0.00	0.00	0.09	**0.00**	**0.00**	0.14	0.03	100.86	1.58	99.28
17-2	053 a2	3.93	0.03	0.23	0.14	1.11	0.23	0.29	36.07	49.20	0.00	0.01	0.21	**1.39**	**2.60**	0.27	0.07	95.79	1.65	94.14
17-3	053 a2	4.17	0.02	0.11	0.33	0.88	0.02	0.12	36.22	50.35	0.00	0.00	0.12	**0.91**	**2.17**	0.30	0.02	95.75	1.76	94.00
17-4	053 a2	4.04	0.02	0.14	0.00	0.00	0.22	0.00	42.17	54.29	0.00	0.01	0.10	**0.00**	**0.07**	0.09	0.08	101.24	1.70	99.54
17-5	053 a2	4.55	0.03	0.64	0.65	1.42	0.07	0.11	37.07	49.43	0.00	0.00	0.26	**1.13**	**2.30**	0.30	0.20	98.16	1.92	96.24
17-6	053 a2	5.26	0.02	0.27	0.17	0.93	0.17	0.07	36.17	50.76	0.00	0.00	0.14	**0.83**	**1.90**	0.31	0.06	97.06	2.21	94.84

Photomicrographs showing representative textures and the locations of spot analyses of Pb+U-enriched apatite crystals by EMPA (Table G-3).

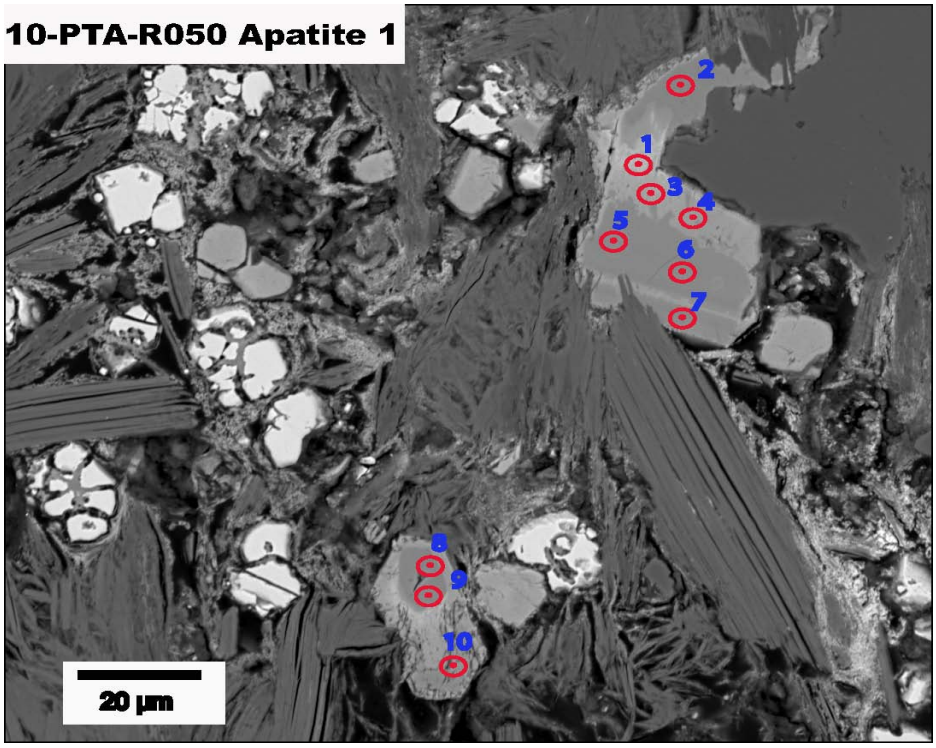

Figure G-10. Abundant disseminated euhedral to subhedral apatite grains (medium to pale grey) interspersed with pyrite (bright) crosscut by limonite network, enclosed in felted illite, all interstitial to and partly replacing muscovite. The numbered dots show the locations of spot analyses by electron microprobe (Table G-3). The pale grey portions of the apatite are enriched in Pb+U. Both apatite phases replace and surround muscovite. Upper right corner is quartz.

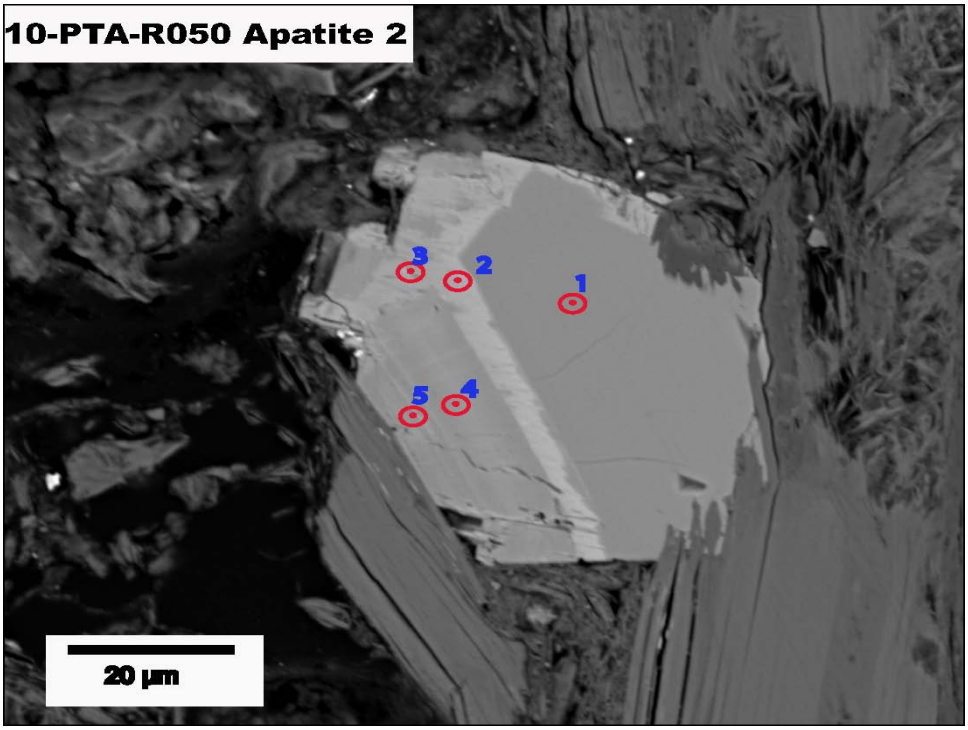

Figure G-11. Apatite that has grown mainly in the interstices of muscovite, which is bent (possibly displaced by apatite growth) and partly replaced by the apatite. Compositional zoning is clearly visible in the apatite crystal; the brighter reflectance (spots 2 and 3) is associated with Pb+U replacing Ca (Table G-3). The matrix of felted illite and chlorite has partly replaced muscovite and the upper right corner of the apatite crystal appears to have been partly overgrown by.

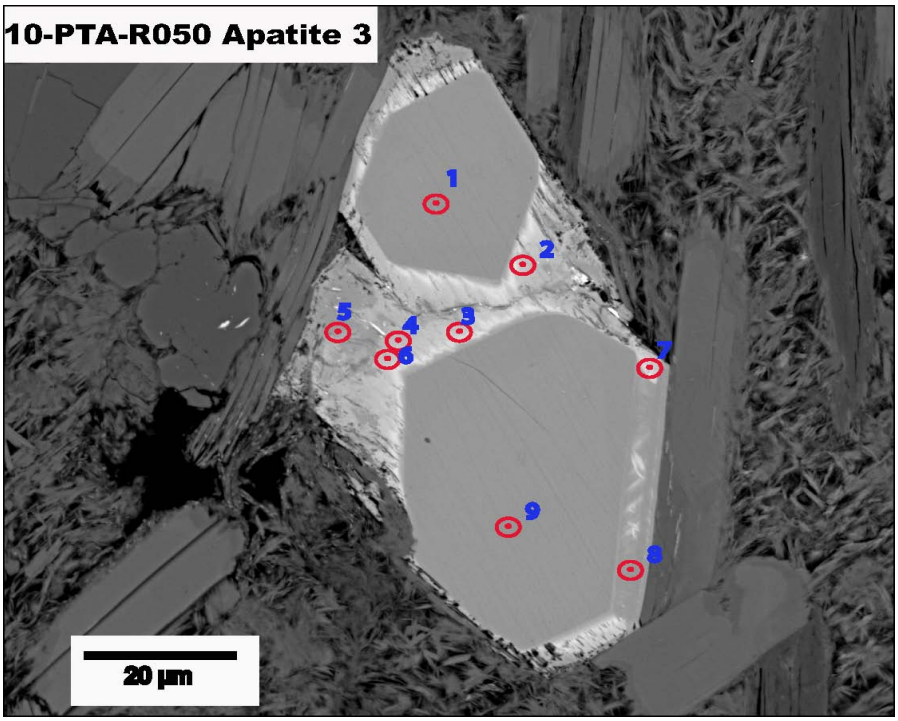

Figure G-12. Apatite displaying chemical zoning from low Pb+U in the centre (spots 1, 9) to high Pb+U in the surrounding overgrowths or alteration of the primary apatite (Table G-3). The matrix comprises minor quartz and feldspar and a felted mass of illite and chlorite and is interstitial to distinct tabular-appearing muscovite plates that partly constrained the apatite growth and are interpreted as relicts of the pre-alteration metamorphic assemblage. Figures G-13, G-14, and G-15 show X-ray images of the apatite crystals, which highlight the compositional variations in Pb, U, and Ca, respectively. Quartz in middle left.

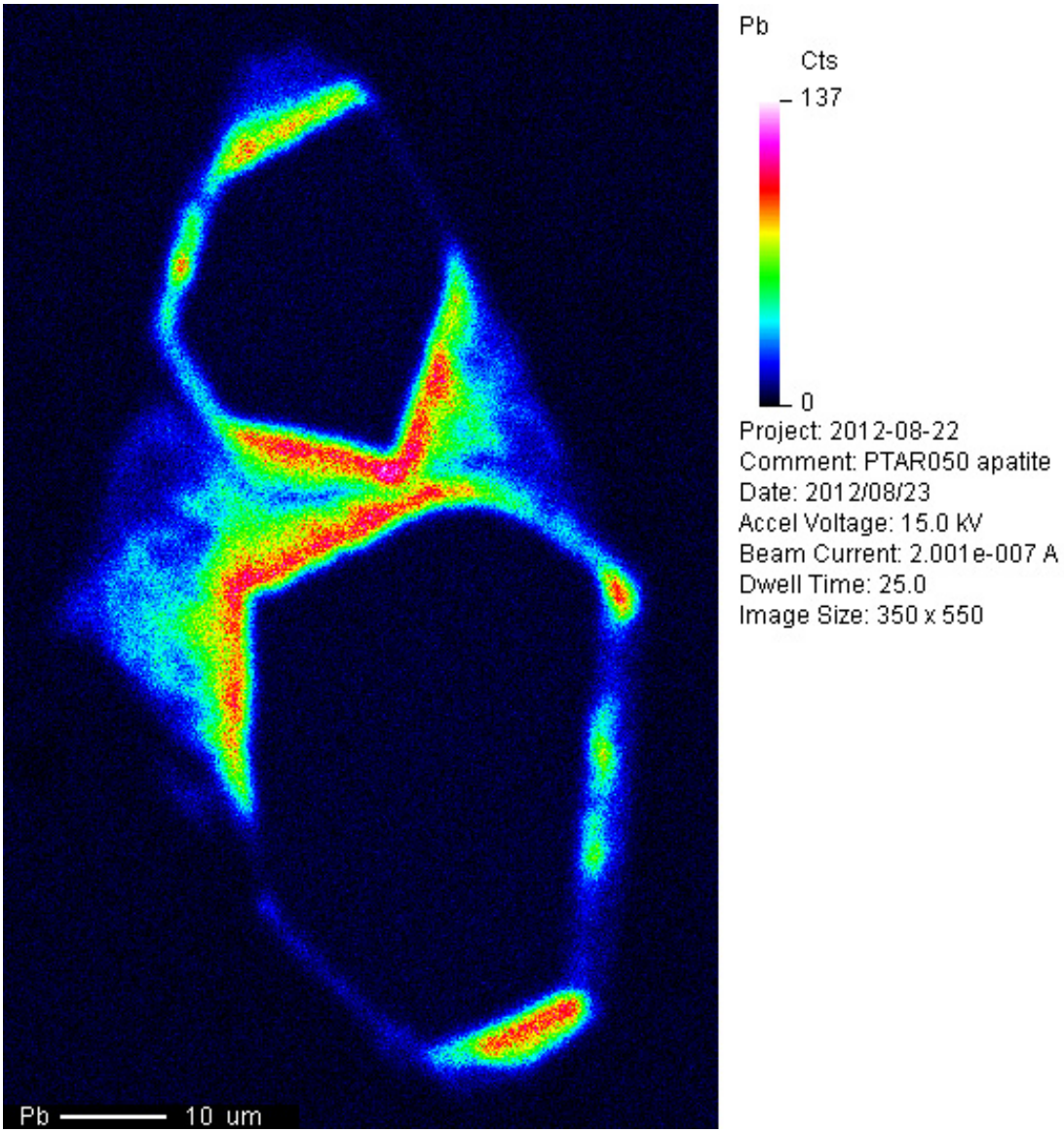

Figure G-13. 10-PTA-R050 Apatite 3. X-ray image clearly displays the location of elevated Pb that, along with U, takes the place of Ca in the apatite phase that overgrew or replaced the original core apatite crystals (dark). This details the same apatite crystals as are shown in Figures G-12 and G-14.

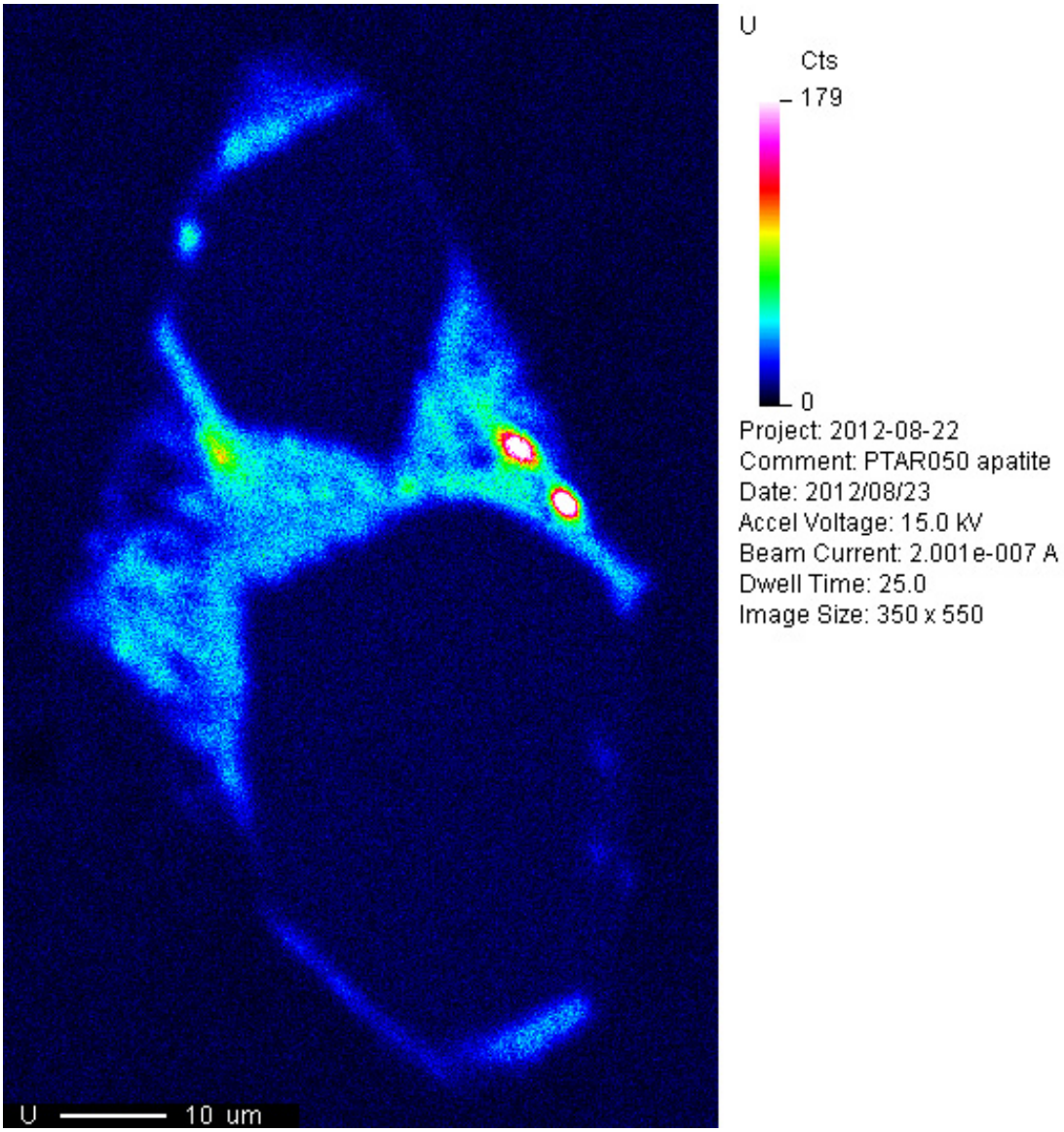

Figure G-14. 10-PTA-R050 Apatite 3. X-ray image illustrating the elevated U zones, roughly coincident with Pb, in apatite that replaced or overgrew the original apatite as shown in Figures G-12 and G-13.

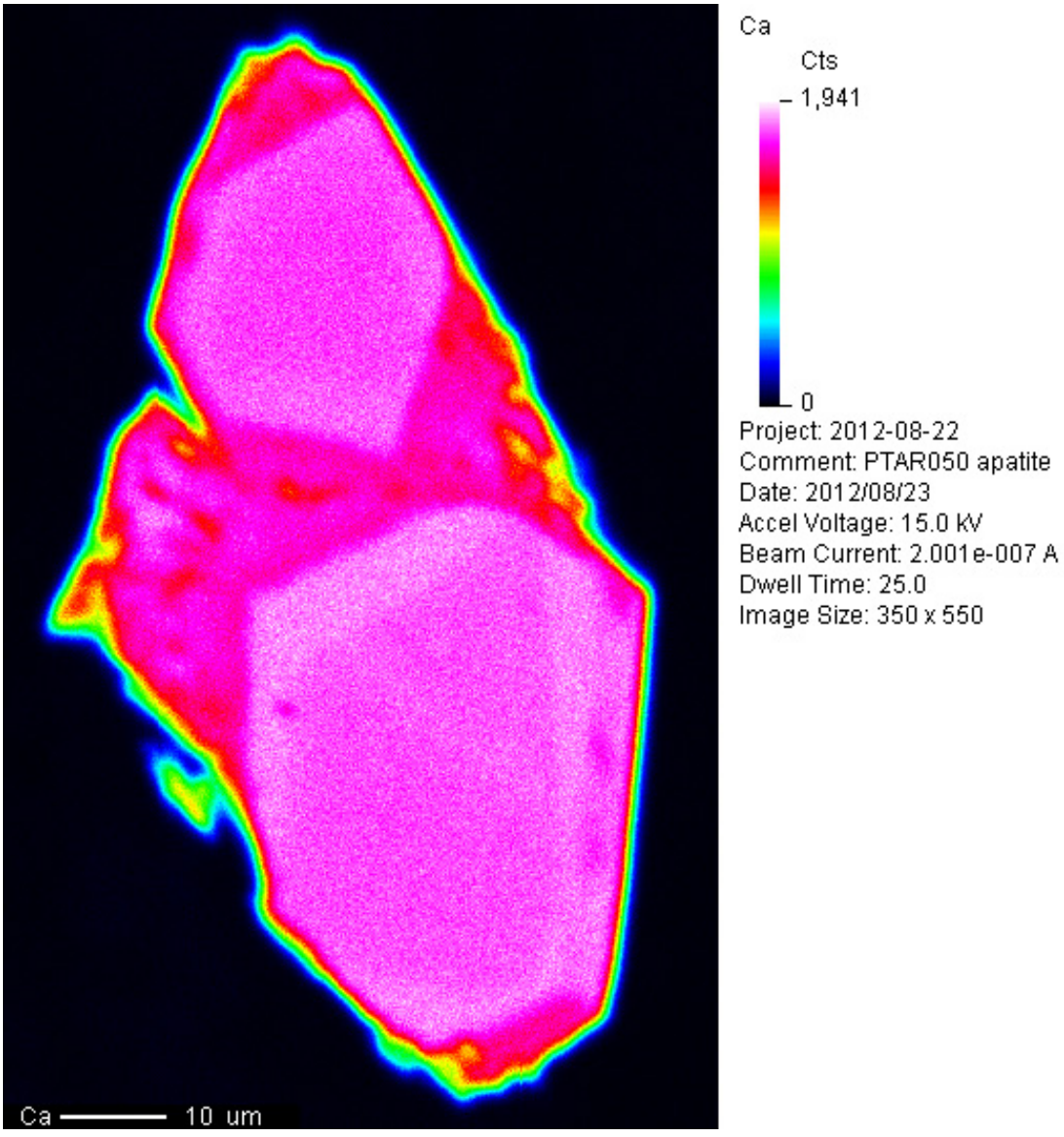

Figure G-15: 10-PTA-R050 Apatite 3. X-ray image illustrating the compositional zonation of Ca, which sharply decreases within the exterior 'rim' that connects the two primary, Ca-rich apatite crystals. Same field of view as is shown in Figures G-13 and G-14 and details the same crystals shown in context in Figure G-12.

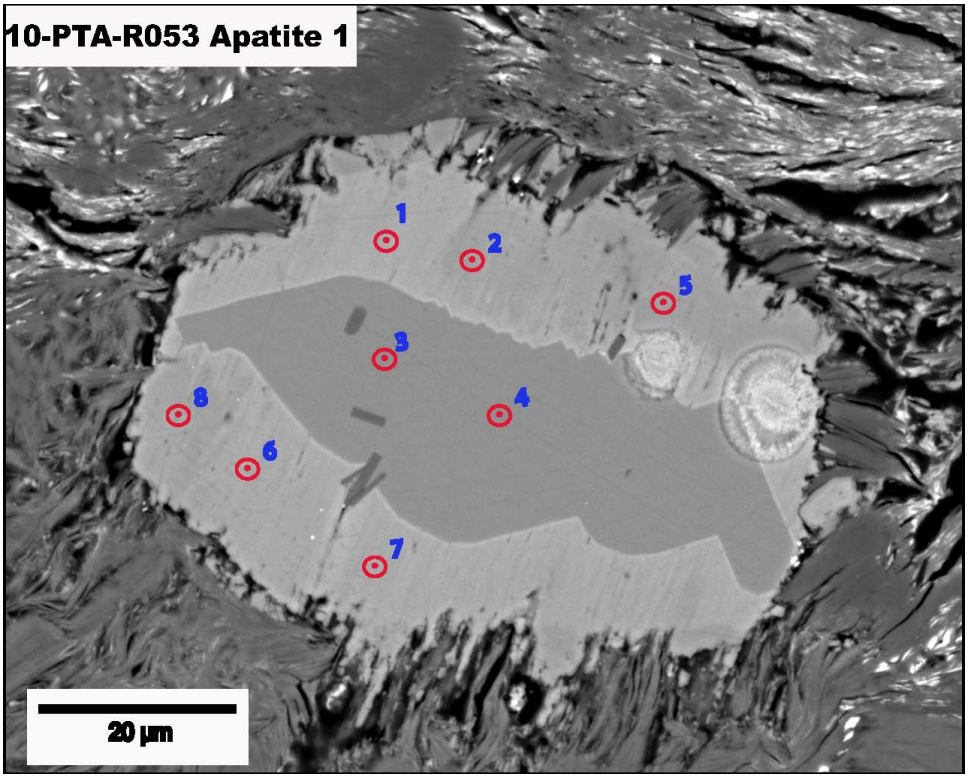

Figure G-16. An apatite crystal, with a wide Pb+U enrichment zone, is in optical continuity with the apatite and interdigitated along its outer margin with highly altered muscovite or illite, with minor replacement uraninite and illite. Note micron-sized laths of muscovite that are included in the inner primary apatite and are retained in the outer Pb+U enriched apatite. The enclosing matrix of felted illite and chlorite has a random fabric below the apatite and is oriented parallel to the diagonal laminae in the Pb+U enriched apatite (lower left to upper right), yet trends from left to right in the uranium-rich illite across the top of the view, thus recording different structural domains within this mineralization assemblage. The Pb+U enrichment propagated only in the direction of the diagonal lamellae.

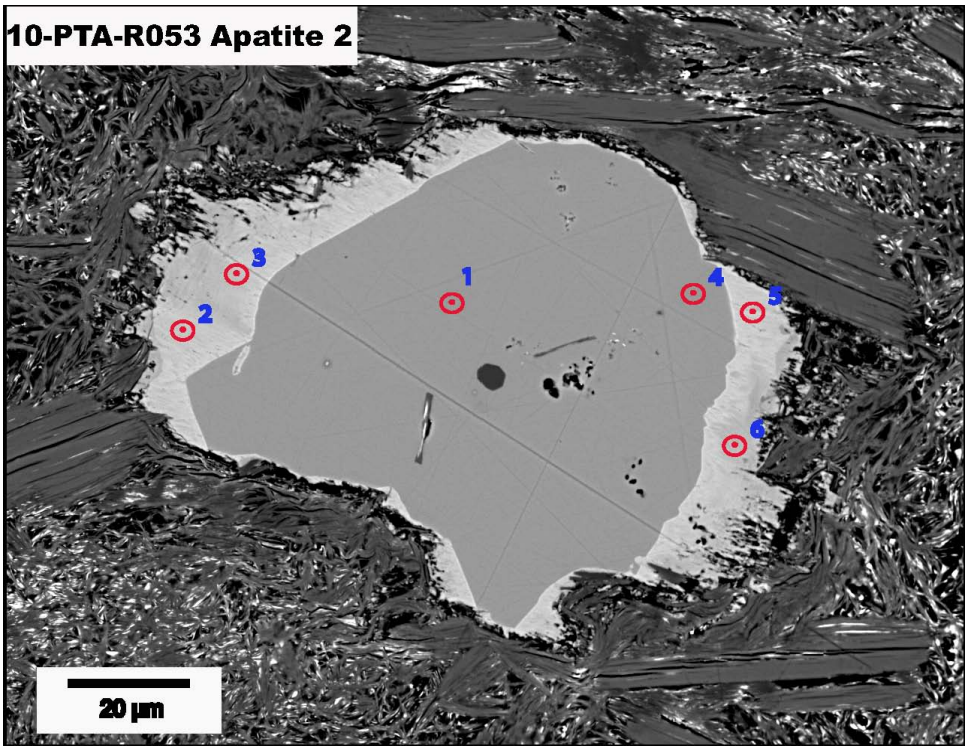

Figure G-17. Apatite displaying clear textural evidence of replacing muscovite around its upper right margin, and of being replaced outboard by Pb+U enriched apatite that is interdigitated with matrix felted illite-uraninite-galena. The Pb+U enrichment zone has a fine oblique lamination (upper left to lower right) that is perpendicular to the direction of propagation (as in Fig. G-16) and is much narrower where the apatite crystal abuts muscovite.

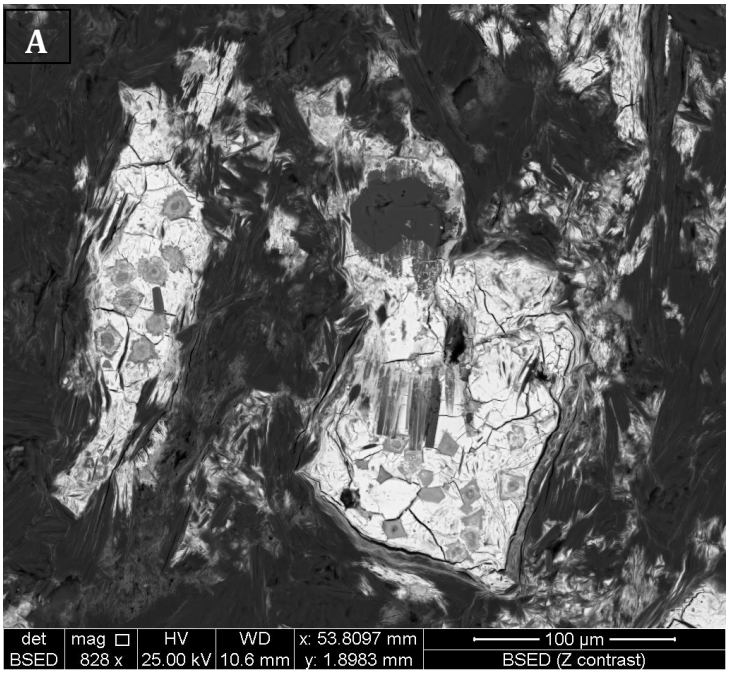

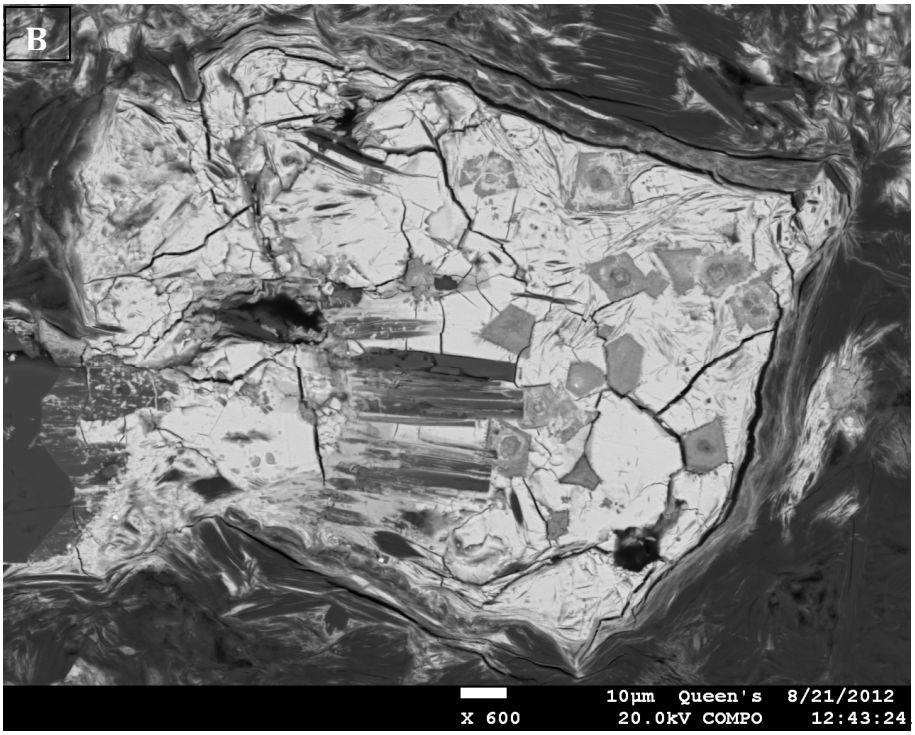

Figure G-18. 10-PTA-R053.SEM backscatter image of uraninite crystals (bright) enclosing relict 4- to 6-sided concentrically zoned pyrite framboids and pre-existing muscovite; set in a matrix of intergrown illite, chlorite, and uraninite. Note the preferred structural orientation of all phases from lower left to upper right, with exception of the illite-chlorite that wraps around the immediate margins of the larger uraninite crystal. Dark isotropic mineral in upper centre are wrapped by uraninite is quartz. (A) Overall view; (B) Detail of larger uraninite crystal, rotated 90° counterclockwise.

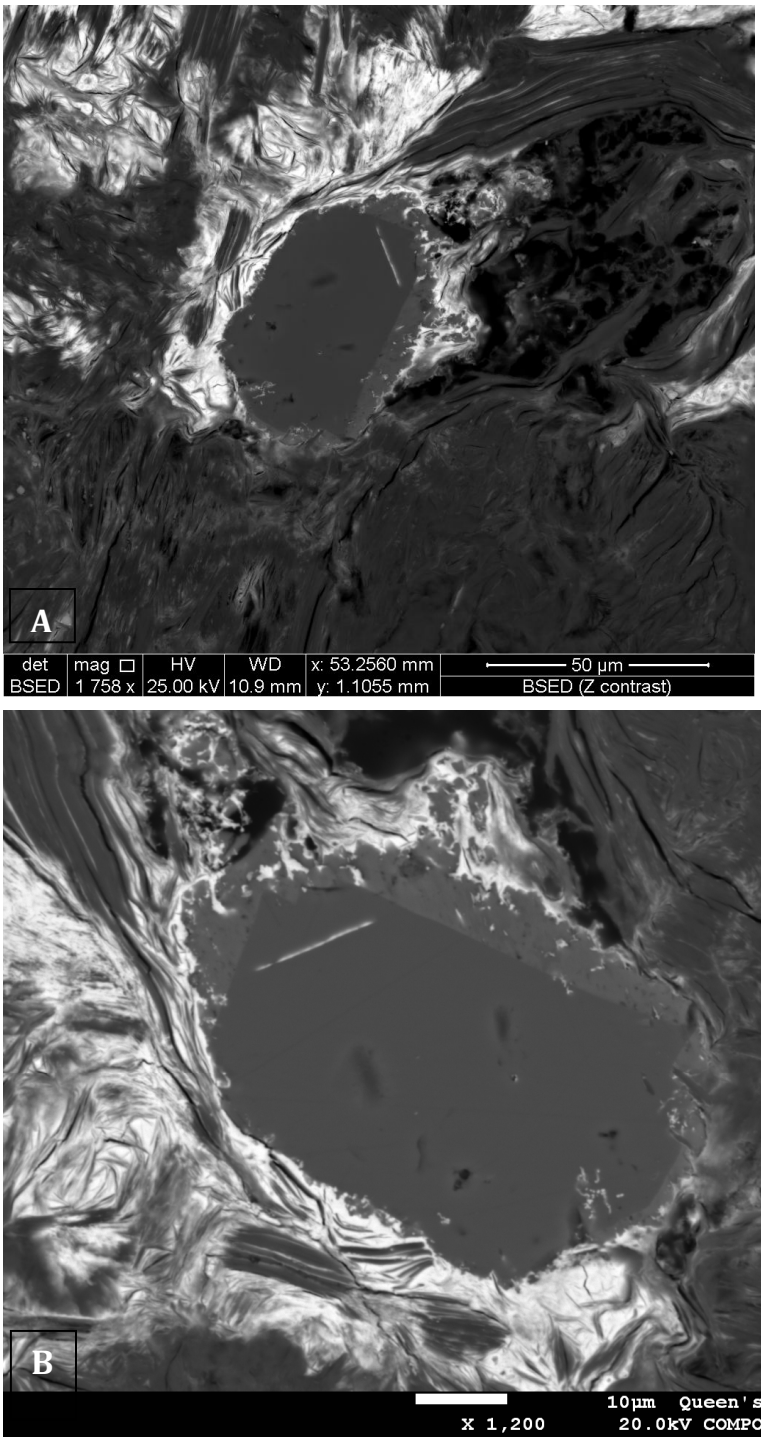

Figure G-19. SEM backscatter image of apatite (uniform medium grey) with an asymmetric and ragged Pb+U enriched rim, partially surrounded by uraninite-rich illite+chlorite matrix; the balance of the phyllosilicates are low in U. Note the greater thickness of the enriched apatite rim in the same direction as the alignment of the phyllosilicate minerals (lower left to upper right in (A)). B) Detail of the apatite crystal shown in (A), rotated 90° counter-clockwise.